


Phase slips and parity jumps in quantum oscillations of inverted InAs/GaSb quantum wells

Matija Karalic,^{*} Christopher Mittag, Susanne Mueller, Thomas Tschirky,
Werner Wegscheider, Klaus Ensslin, and Thomas Ihn
Solid State Physics Laboratory, ETH Zurich, 8093 Zurich, Switzerland

Leonid Glazman
Department of Physics, Yale University, New Haven, Connecticut 06520, USA

 (Received 21 September 2018; revised manuscript received 28 January 2019; published 3 May 2019)

We present magnetotransport measurements of a strongly hybridized inverted InAs/GaSb double quantum well. We find that the spin-orbit interaction leads to an appreciable spin-splitting of hole-like states, which form distinct Landau levels in a perpendicular magnetic field. The resulting quantum Hall state is governed by a periodic even and odd total filling arising due to the simultaneous occupation of electron-like and hole-like Landau levels of differing degeneracy. Furthermore, oscillatory charge transfer between all involved subbands leads to discrete phase slips in the usual sequential filling of Landau levels, and coincidentally the phase slips are close to π . These results shed light on the Landau level structure in composite systems and have consequences for interpreting intercepts obtained from index plots, which are routinely employed to investigate the presence of Berry's phase.

DOI: [10.1103/PhysRevB.99.201402](https://doi.org/10.1103/PhysRevB.99.201402)

Quantum oscillations arise in the electronic transport in metals and semiconductors in a magnetic field and provide insights into the physical properties of the system under investigation. At low fields, Shubnikov–de Haas (SdH) oscillations reveal the densities of the charge carriers present, as well as the degeneracy (spin, valley) of the Landau levels (LLs) that result from the quantization of motion in the magnetic field. At higher fields the quantum Hall (QH) effect may develop, leading to quantization in the Hall resistivity. Understanding the electronic structure in magnetic fields becomes an essential undertaking whenever a new material system is discovered. For instance, one of the major results accompanying the first successful exfoliation of graphene was the half-integer QH effect [1,2]. Furthermore, quantum oscillations were used to infer the nontrivial Berry's phase of massless Dirac fermions.

InAs/GaSb double quantum wells (QWs) are a composite system characterized by the hybridization of electrons and holes. Hybridization may result in a nontrivial band structure [3–8], making this system a platform for the realization of the quantum spin Hall insulator [9–14]. Here, we report on the LL structure in an inverted InAs/GaSb double QW and critically discuss the determination of Berry's phase from quantum oscillations.

We uncover a periodic even and odd filling of LLs leading to a checkerboard pattern in the longitudinal resistivity, reminiscent of recent observations in transition metal dichalcogenides (TMDCs) [15–17]. We go on to explain how the combination of spin-orbit interaction (SOI) and Landau quantization can lead to an unconventional occupation sequence of LLs. Additionally, we discover an anomalous shift which

violates the usual $1/B_{\perp}$ -periodic sequence of LL filling. This shift is synonymous with discrete phase slips in the quantum oscillations. A fundamental consequence of the phase slips is that the intercept γ for $1/B_{\perp} \rightarrow 0$ in an index plot $\nu(1/B_{\perp})$, where ν is the filling factor, is not meaningful for evaluating Berry's phase. We compare this finding to experiments on other two- and three-dimensional (2D/3D) systems.

Measurements were performed on a gated Hall bar of 10 μm width and 20 μm length oriented along the $[0\bar{1}1]$ crystallographic direction on a heterostructure consisting of an 8 nm GaSb QW and a 13.5 nm InAs QW [Fig. 1(a)]. All measurements were conducted in a dilution refrigerator at a base temperature of 135 mK using low-frequency lock-in techniques with constant current bias.

The inverted band structure of our double QW is schematically depicted in Fig. 1(b). The InAs QW thickness is sufficiently large to drive the system into the semimetallic phase. This implies enhanced hybridization between electron and hole bands, while the anisotropy of the dispersion effectively quenches the hybridization gap. The Rashba-type SOI already present in the constituent QWs is amplified by the hybridization, and leads to significant splitting of valence and conduction bands [18–22]. The longitudinal resistivity ρ_{xx} , see Fig. 1(c), shows no local resistance maximum at or close to the charge neutrality point (CNP), indicating the lack of a true energy gap, as expected [23]. In the shaded area in Fig. 1(b) between the CNP and the former top of the GaSb valence band both electrons (majority) and holes (minority charge carriers) are present. This region is probed in the following.

Figure 1(d) shows a map of ρ_{xx} as a function of top gate voltage V_{tg} and perpendicular magnetic field B_{\perp} . The voltage V_{tg} tunes the total charge carrier density in the system. Two

^{*}makarali@phys.ethz.ch

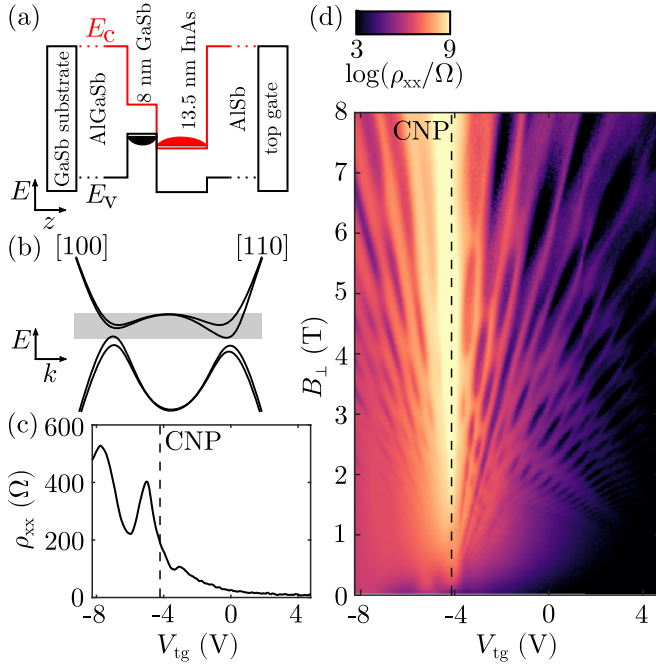


FIG. 1. (a) Conduction (valence) band edge energy E_c (E_v) as a function of growth direction z for the InAs/GaSb system. (b) Schematic band structure $E(k)$ of the double QW system. The shaded area is investigated in subsequent experiments. (c) ρ_{xx} at $B_{\perp} = 0$ as function of V_{tg} with the position of the CNP highlighted. (d) ρ_{xx} as function of V_{tg} and B_{\perp} with the position of the CNP highlighted.

sets of lines fanning outward from the CNP follow minima in ρ_{xx} . Remarkably, we discern an atypical yet regular pattern in the distribution of minima. Minima in ρ_{xx} of constant filling are modulated, moving toward and away from zero resistivity in a systematic fashion depending on their position in the (V_{tg}, B_{\perp}) space. We focus on the region to the right of the CNP where electrons are in the majority and discuss the properties and origins of the observed checkerboard pattern.

The region of interest in Fig. 1(d) is reproduced in Fig. 2(a) for clarity. Figure 2(b) is a cut at constant total density at $V_{tg} = 3V$, showing both longitudinal and transverse resistivities ρ_{xx} and ρ_{xy} versus $1/B_{\perp}$. Well-developed plateaus are described by $\rho_{xy} = h/\nu e^2$ with integer ν and occur concomitantly with minima in ρ_{xx} . Because we probe a composite system with multiple charge carrier species, ν corresponds to a total filling factor, taking both electron- and hole-like LLs into account [24]. While minima typically do not reach zero, the quantization in ρ_{xy} suffices for an unambiguous assignment of ν . Looking at the sequence of plateaus in ρ_{xy} , we deduce that ν decreases in increments of two with $1/B_{\perp}$, with the exception of selected transitions indicated by the dotted lines. There, ν changes by one only. This way, the parity of ν switches between even (denoted by stars) and odd (circles) as a function of magnetic field. The positions of the minima in ρ_{xx} at $V_{tg} = 3V$ are also marked by symbols in Fig. 2(a). The minima in ρ_{xx} corresponding to the missing plateaus are suppressed. Using the quantization of ρ_{xy} , we assign a filling factor to each minimum and highlight minima of even and odd ν in Fig. 2(a) with differently colored contour lines. We

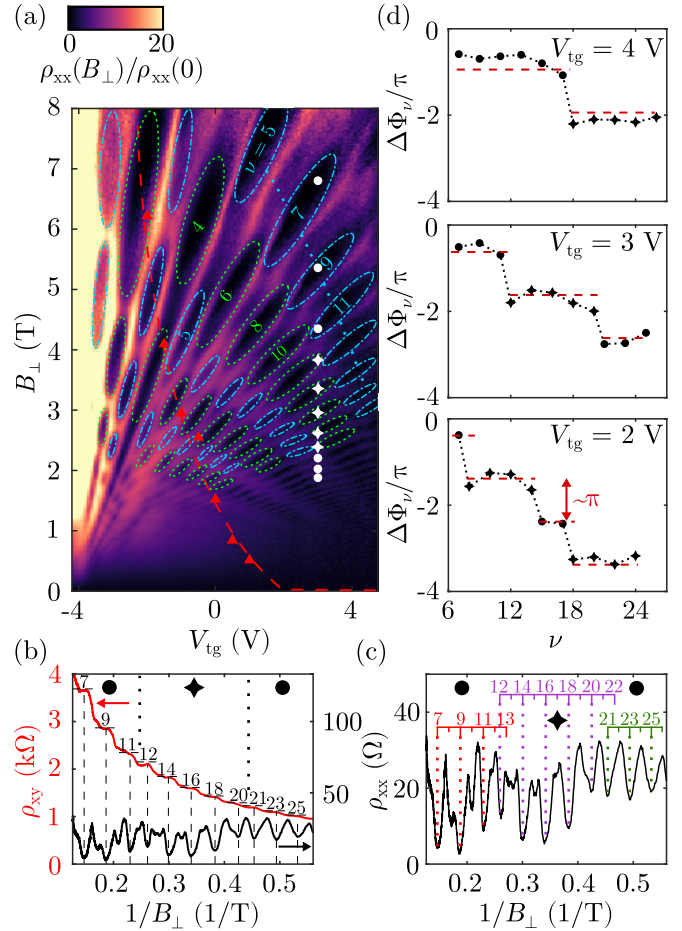


FIG. 2. (a) Zoom-in of Fig. 1(d). Contour lines marking minima associated with either even or odd total filling factor ν are colored differently, with ν given explicitly for some minima. The dotted line connecting several minima of odd parity exemplifies how adjacent minima of the same parity lie on lines of negative slope. Circles (stars) mark positions of odd (even) ν minima at $V_{tg} = 3V$ as in (b), (c), (d). Triangles and the dashed line serving as a guide to the eye correspond to the situation where the density p_2 , as introduced in the main text, equals eB_{\perp}/h . (b) ρ_{xx} , ρ_{xy} as function of $1/B_{\perp}$ at $V_{tg} = 3V$ with positions of minima in ρ_{xx} and expected positions of plateaus in ρ_{xy} , h/ie^2 with integer i , marked by dashed lines. Associated $\nu = i$ are also indicated. (c) ρ_{xx} reproduced from (b) with minima marked by dotted lines and rulers associated with each segment of constant parity of ν showing the expected positions of minima and the affiliated values of ν . (d) Steps in the oscillations' phase as a function of ν for several values of V_{tg} , see main text for details. Horizontal dashed lines spaced by $\Delta\Phi_{\nu} = \pi$ provide a guide to the eye.

observe that neighboring minima of the same parity seemingly lie on lines of negative slope, as illustrated by the dotted line. A cut at fixed V_{tg} such as in Fig. 2(b) typically intersects multiple such lines, so that minima correspond to ν being piecewise even or odd. The pattern apparently changes upon approaching the CNP, becoming more complex. Similar even-odd behavior in TMDCs was attributed to interplay between cyclotron and Zeeman energies and to a density-dependent g factor [15–17]. We also observed faint signs of said behavior in weakly inverted InAs/GaSb double QWs, erroneously

attributing it only to avoided crossings between LLs mediated by ordinary and spin-orbit interband coupling effects [7].

In addition to the unconventional filling sequence, there exists another peculiarity in the form of discrete phase slips occurring whenever the parity switches. Figure 2(c) depicts $\rho_{xx}(1/B_{\perp})$, again at $V_{\text{tg}} = 3\text{V}$. Starting from low $1/B_{\perp}$, we see that the minima corresponding to $\nu = 7, 9, 11$ are equidistantly spaced in $1/B_{\perp}$. However, the subsequent $\nu = 12$ minimum is not located at the expected position, but instead halfway between where the $\nu = 12$ and $\nu = 13$ would lie according to the periodicity set by the $\nu = 7, 9, 11$ minima. The same phenomenon repeats itself at higher $1/B_{\perp}$ at the transition from even to odd ν . There, the $\nu = 21$ minimum lies halfway between the nonexistent $\nu = 21$ and $\nu = 22$ minima which would follow the periodicity determined by the observed $\nu = 12\text{--}20$ minima. The period in $1/B_{\perp}$ remains approximately constant regardless of the shifts. We have verified that the shifts occur generically for all $(V_{\text{tg}}, B_{\perp})$ shown in Fig. 2(a) whenever the parity of ν changes.

We may describe the shifts in terms of discrete phase slips. To quantify the phase slips, we extract an average total density n_{QHE} of charge carriers in the QH state by piecewise fitting of $\nu(1/B_{\perp})$ in an index plot for fixed V_{tg} [25]. Then, we calculate the phase slip $\Delta\Phi_{\nu}/\pi$ using $\Delta\Phi_{\nu}/\pi = 2\hbar n_{\text{QHE}}\Delta(1/B_{\perp})/e$, where $\Delta(1/B_{\perp})$ is the difference in $1/B_{\perp}$ between the expected position of the minimum corresponding to ν , $e\nu/\hbar n_{\text{QHE}}$, and the position where it actually occurs. Figure 2(d) presents the evolution of $\Delta\Phi_{\nu}/\pi$ for several V_{tg} . The phase is seen to jump downward by around π whenever the parity switches.

To understand the origin of the even-odd periodicity and the phase slips, we investigate the densities of all charge carriers, as displayed in Fig. 3 [25]. The low-field SdH oscillations exhibit a single frequency f_2 for $V_{\text{tg}} > 2.5\text{V}$ which decreases upon decreasing V_{tg} and therefore corresponds to electron-like states. The frequency f_2 is related to the Hall density n_{tot} obtained from fitting ρ_{xy} above a certain B_{\perp} value where ρ_{xy} is linear in B_{\perp} through $n_{\text{tot}} \approx 2f_2 \times e/h$. Because n_{tot} determined in this way measures the total density of free charge carriers, the factor of 2 implies that the population imbalance due to spin-splitting is negligible and that carriers populate a twofold degenerate electron-like band. For $V_{\text{tg}} \leq 2.5\text{V}$, an additional frequency f_1 appears, see Fig. 3(a). The frequency f_1 increases upon decreasing V_{tg} , implying hole-like states. Close to $V_{\text{tg}} = 2.5\text{V}$ we have $n_{\text{tot}} \approx (2f_2 - f_1) \times e/h$, signifying that f_1 describes a single spin-orbit split hole subband. Upon decreasing V_{tg} further a systematic deviation between n_{tot} and $(2f_2 - f_1) \times e/h$ appears, as observed in Fig. 3(b). The frequencies f_1 and f_2 cannot account for all charge carriers, increasingly overestimating the density, $n_{\text{tot}} < (2f_2 - f_1) \times e/h$. This motivates us to look for the second spin-orbit split hole subband containing the missing holes that does not partake in SdH oscillations. We therefore fit ρ_{xx} and ρ_{xy} simultaneously with a three-band model by inverting $\sigma_{xx} = \sum \sigma_{xx}^i$ and $\sigma_{xy} = \sum \sigma_{xy}^i$ with $\sigma_{xx}^i, \sigma_{xy}^i$ being the conductivities of the individual bands ($i = 1, 2, 3$). We fix two of the three densities to $p_1 = f_1 \times e/h$ and $n = 2f_2 \times e/h$, respectively, leaving four fitting parameters, namely, p_2 , the missing density, and three mobilities μ_i [25]. The complete result for all V_{tg} is shown in Fig. 3(c). Three-band fitting

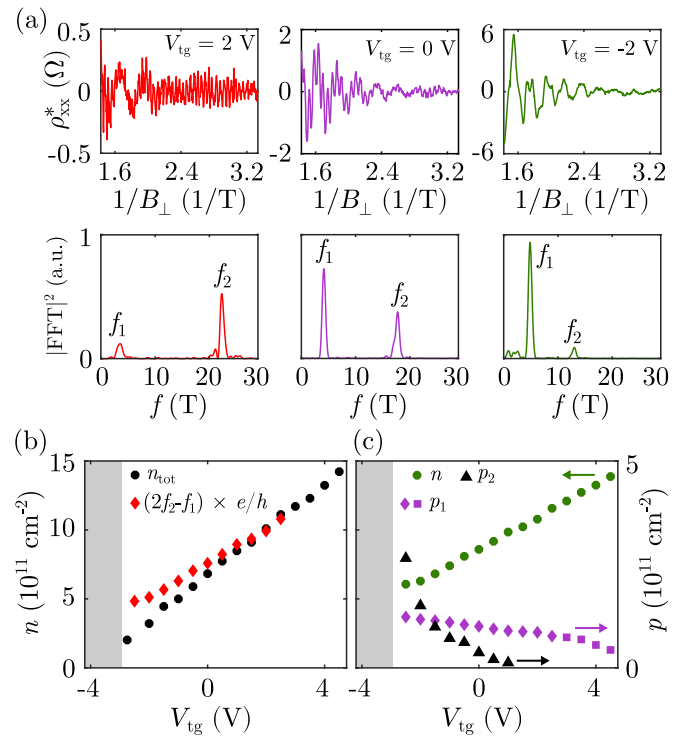


FIG. 3. (a) Exemplary low-field SdH oscillations after background subtraction with the corresponding normalized power spectra for several V_{tg} . (b) Hall density n_{tot} and the total density $(2f_2 - f_1) \times e/h$ obtained from the SdH oscillations as function of V_{tg} . In the shaded region, reliable data points are lacking. (c) As in (b), but showing n , the electron density, as well as p_1 and p_2 , the densities of the spin-split hole subbands. p_1 is determined from SdH oscillations (diamonds) and two-band fitting (squares).

works for $V_{\text{tg}} \leq 1\text{V}$. For $V_{\text{tg}} > 1\text{V}$, p_2 is too small compared to p_1 and n to be determined reliably and a two-band model sufficiently describes the data, resulting in densities that agree with p_1 and n as defined above for $1 < V_{\text{tg}} \leq 2.5\text{V}$. For $V_{\text{tg}} > 2.5\text{V}$ a two-band fit allows us to determine the continuation of p_1 where f_1 disappears from the SdH oscillations.

We found that the spin-splitting of the electron-like band of density n cannot be experimentally resolved. The same is true for the conventional Zeeman splitting of this band [26]. Hole-like states exist in two subbands and have different dispersions due to the SOI, and therefore Landau quantization of each results in nondegenerate levels. The hole-like subband of density p_1 enters the QH state, whereas the subband of density p_2 does not. Above the dashed line in Fig. 2(a), $p_2 < eB_{\perp}/h$, being insufficient to change the total filling factor by one, and we may think of these holes as forming a background density.

The dispersion of LLs close to a (anti)crossing point between twofold degenerate electron-like and nondegenerate hole-like levels is schematically depicted by lines in Fig. 4(a) together with ν_e and ν_h , the filling factors of the electron- and hole-like levels, respectively ($\nu = \nu_e - \nu_h$). Filling factors ν_e are even and change in increments of two, whereas ν_h is even or odd and changes in increments of one. Converting from (E, B_{\perp}) to $(V_{\text{tg}}, B_{\perp})$, we obtain the diagram in Fig. 4(b), recognizing the even-odd pattern. The hole mass being larger

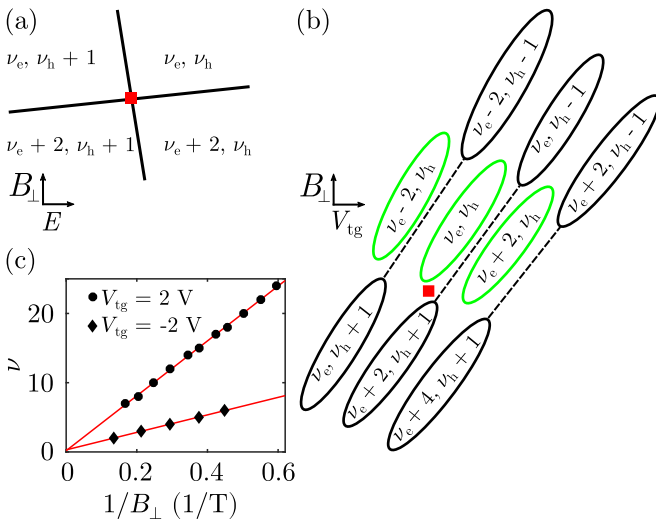


FIG. 4. (a) Filling of LLs in (E, B_{\perp}) space in the vicinity of a crossing point between a doubly degenerate electron-like LL and a nondegenerate hole-like LL of corresponding filling ν_e and ν_h , respectively. (b) As in (a), but upon conversion to $(V_{\text{tg}}, B_{\perp})$ space. The crossing point from (a) is now located at the position indicated by the square. Dashed lines connect minima of constant ν . (c) Index plots demonstrating the extrapolation of ν for $1/B_{\perp} \rightarrow 0$ at $V_{\text{tg}} = 2\text{V}$ and -2V .

than the electron mass explains why typically several electron-like LLs are depopulated before a hole-like LL is depopulated for constant V_{tg} . A simple density of states model confirms this picture [25].

The electrochemical potential μ_{elch} oscillates as a function of B_{\perp} at constant *total* density for fixed V_{tg} . However, the densities of the individual subsystems also oscillate together with μ_{elch} . The phase slips occur because the density of charge carriers in the QH state, n_{QHE} , is not constant due to the self-consistent charge transfer between the electron- (n) and hole-like states (p_1) in the QH state and the hole-like states constituting the background charge reservoir (p_2). Because the charge transfer is particularly favorable whenever μ_{elch} jumps between hole LLs, that is where the phase slips occur. The phase slips reflect the fact that the points in the index plot $\nu(1/B_{\perp})$ do not all lie on a single line. The index plot is only piecewise linear, as highlighted in the Supplemental Material [25], with shifts in $1/B_{\perp}$ wherever the parity jumps. Each horizontal shift in $1/B_{\perp}$ is equivalent to a phase slip of around π . While the deviation of the points from a single line is easily overlooked [Fig. 4(c)], it unveils itself dramatically when looking at ρ_{xx} traces [Fig. 2(c)] or at the phases of the oscillations [Fig. 2(d)].

In 2D systems in which the total density n_{QHE} of charge carriers quantized in a magnetic field is constant, μ_{elch} is a

function of B_{\perp} . Then, the intercept γ for $1/B_{\perp} \rightarrow 0$ in an index plot must *always* be either 0 or $1/2$ [27]. A nontrivial intercept $\gamma = 1/2$ reflects the existence of a LL at zero energy, as in graphene, whereas a trivial $\gamma = 0$ reflects the lack thereof, independent of the zero-field spectrum. Since a zero energy LL may be viewed as a consequence of a nontrivial Berry's phase of π , $\gamma = 1/2$ was used in graphene to infer the nontrivial Berry's phase of massless Dirac fermions [1,2]. In 3D topological insulators (TIs), the situation is different. The electrochemical potential is pinned by localized states in the bulk (whose number scales with the volume), so the 2D density at the conducting surfaces may vary, while μ_{elch} is fixed. Then, γ may take on nontrivial values between 0 and $1/2$, reflecting Berry's phase [27–31].

There are experimental reports in the literature on 2D systems where $n_{\text{QHE}} = \text{const}$ should hold, yet a nontrivial γ was seen and linked to Berry's phase. Examples include HgTe [32] and InAs/GaSb double QWs [21]. In the latter Ref. [21], a nontrivial intercept $0 < \gamma < 1/2$ was reported close to the CNP and interpreted as originating from a nonzero Berry's phase. We also find a nontrivial γ close to the CNP ($\gamma = 0.30 \pm 0.05$ at $V_{\text{tg}} = -2\text{V}$) and a trivial $\gamma \approx 0$ away from the CNP ($\gamma = 0.18 \pm 0.17$ at $V_{\text{tg}} = 2\text{V}$), see Fig. 4(c). However, taking a single, common intercept is not a meaningful approach since the index plot is piecewise linear. Away from the CNP, $\gamma \approx 0$ due to averaging over the piecewise linear segments in the index plot. This is exemplified in the Supplemental Material [25]. Therefore, attributing nonzero intercepts to a nontrivial Berry's phase is not justified here. When both n_{QHE} and μ_{elch} depend on B_{\perp} , utmost care is required in interpreting γ .

In summary, electron-hole hybridization and the SOI lead to an even-odd periodicity upon Landau quantization. Electron- and hole-like LLs have different degeneracies, leading to parity jumps. Clandestine hole-like states that do not directly appear in quantum oscillations nevertheless have a profound impact, causing abrupt phase slips in the usual $1/B_{\perp}$ -periodic sequence of LLs due to intersubband charge transfer. This phenomenon can lead to nontrivial intercepts obtained from index plots which are not associated with a nontrivial Berry's phase. Our findings are not specific to InAs/GaSb double QWs, but also apply to other 2D and quasi-2D systems which show appreciable SOI or are composite (multiband) in nature, so that they may not fully quantize in a magnetic field, such as HgTe QWs [32,33], TMDCs [34,35], layered pnictides [36], few-layer black phosphorous [37], and 3D TI thin films and nanoribbons [38–40].

The authors thank Andrea Hofmann for discussions and acknowledge the support of the ETH FIRST laboratory and the financial support of the Swiss Science Foundation (Schweizerischer Nationalfonds, NCCR QSIT). L.G. acknowledges the support of NSF DMR Grant No. 1603243.

- [1] K. S. Novoselov, A. K. Geim, S. V. Morozov, D. Jiang, M. I. Katsnelson, I. V. Grigorieva, S. V. Dubonos, and A. A. Firsov, *Nature* **438**, 197 (2005).
 [2] Y. Zhang, Y.-W. Tan, H. L. Stormer, and P. Kim, *Nature* **438**, 201 (2005).

- [3] M. Lakrimi, S. Khym, R. J. Nicholas, D. M. Symons, F. M. Peeters, N. J. Mason, and P. J. Walker, *Phys. Rev. Lett.* **79**, 3034 (1997).
 [4] M. J. Yang, C. H. Yang, B. R. Bennett, and B. V. Shanabrook, *Phys. Rev. Lett.* **78**, 4613 (1997).

- [5] L. J. Cooper, N. K. Patel, V. Drouot, E. H. Linfield, D. A. Ritchie, and M. Pepper, *Phys. Rev. B* **57**, 11915 (1998).
- [6] F. Qu, A. J. A. Beukman, S. Nadj-Perge, M. Wimmer, B.-M. Nguyen, W. Yi, J. Thorp, M. Sokolich, A. A. Kiselev, M. J. Manfra, C. M. Marcus, and L. P. Kouwenhoven, *Phys. Rev. Lett.* **115**, 036803 (2015).
- [7] M. Karalic, S. Mueller, C. Mittag, K. Pakrouski, Q. S. Wu, A. A. Soluyanov, M. Troyer, T. Tschirky, W. Wegscheider, K. Ensslin, and T. Ihn, *Phys. Rev. B* **94**, 241402(R) (2016).
- [8] M. Karalic, C. Mittag, T. Tschirky, W. Wegscheider, K. Ensslin, and T. Ihn, *Phys. Rev. Lett.* **118**, 206801 (2017).
- [9] C. Liu, T. L. Hughes, X.-L. Qi, K. Wang, and S.-C. Zhang, *Phys. Rev. Lett.* **100**, 236601 (2008).
- [10] I. Knez, R.-R. Du, and G. Sullivan, *Phys. Rev. Lett.* **107**, 136603 (2011).
- [11] K. Suzuki, Y. Harada, K. Onomitsu, and K. Muraki, *Phys. Rev. B* **87**, 235311 (2013).
- [12] I. Knez, C. T. Rettner, S.-H. Yang, S. S. P. Parkin, L. Du, R.-R. Du, and G. Sullivan, *Phys. Rev. Lett.* **112**, 026602 (2014).
- [13] S. Mueller, A. N. Pal, M. Karalic, T. Tschirky, C. Charpentier, W. Wegscheider, K. Ensslin, and T. Ihn, *Phys. Rev. B* **92**, 081303(R) (2015).
- [14] L. Du, I. Knez, G. Sullivan, and R.-R. Du, *Phys. Rev. Lett.* **114**, 096802 (2015).
- [15] H. C. P. Movva, B. Fallahazad, K. Kim, S. Larentis, T. Taniguchi, K. Watanabe, S. K. Banerjee, and E. Tutuc, *Phys. Rev. Lett.* **118**, 247701 (2017).
- [16] S. Larentis, H. C. P. Movva, B. Fallahazad, K. Kim, A. Behroozi, T. Taniguchi, K. Watanabe, S. K. Banerjee, and E. Tutuc, *Phys. Rev. B* **97**, 201407(R) (2018).
- [17] R. Pisoni, A. Kormányos, M. Brooks, Z. Lei, P. Back, M. Eich, H. Overweg, Y. Lee, P. Rickhaus, K. Watanabe, T. Taniguchi, A. Imamoglu, G. Burkard, T. Ihn, and K. Ensslin, *Phys. Rev. Lett.* **121**, 247701 (2018).
- [18] A. Zakharova, S. T. Yen, and K. A. Chao, *Phys. Rev. B* **66**, 085312 (2002).
- [19] J. Li, W. Yang, and K. Chang, *Phys. Rev. B* **80**, 035303 (2009).
- [20] L.-H. Hu, C.-X. Liu, D.-H. Xu, F.-C. Zhang, and Y. Zhou, *Phys. Rev. B* **94**, 045317 (2016).
- [21] F. Nichele, M. Kjaergaard, H. J. Suominen, R. Skolasinski, M. Wimmer, B.-M. Nguyen, A. A. Kiselev, W. Yi, M. Sokolich, M. J. Manfra, F. Qu, A. J. A. Beukman, L. P. Kouwenhoven, and C. M. Marcus, *Phys. Rev. Lett.* **118**, 016801 (2017).
- [22] A. J. A. Beukman, F. K. de Vries, J. van Veen, R. Skolasinski, M. Wimmer, F. Qu, D. T. de Vries, B.-M. Nguyen, W. Yi, A. A. Kiselev, M. Sokolich, M. J. Manfra, F. Nichele, C. M. Marcus, and L. P. Kouwenhoven, *Phys. Rev. B* **96**, 241401(R) (2017).
- [23] A resistance maximum gradually evolves at the CNP upon applying a perpendicular magnetic field B_{\perp} .
- [24] K. Suzuki, K. Takashina, S. Miyashita, and Y. Hirayama, *Phys. Rev. Lett.* **93**, 016803 (2004).
- [25] See Supplemental Material at <http://link.aps.org/supplemental/10.1103/PhysRevB.99.201402> for more details.
- [26] For pure InAs, the ratio of Zeeman and cyclotron energies is ~ 0.26 for $g = 15$ and $m^* = 0.036 \times m_0$. Due to the presence of hole-like Landau levels, the spectrum is denser than expected for pure InAs electron systems.
- [27] A. Y. Kuntsevich, A. V. Shupletsov, and G. M. Minkov, *Phys. Rev. B* **97**, 195431 (2018).
- [28] D.-X. Qu, Y. S. Hor, J. Xiong, R. J. Cava, and N. P. Ong, *Science* **329**, 821 (2010).
- [29] A. A. Taskin and Y. Ando, *Phys. Rev. B* **84**, 035301 (2011).
- [30] J. Xiong, Y. Luo, Y. H. Khoo, S. Jia, R. J. Cava, and N. P. Ong, *Phys. Rev. B* **86**, 045314 (2012).
- [31] A. R. Wright and R. H. McKenzie, *Phys. Rev. B* **87**, 085411 (2013).
- [32] B. Büttner, C. X. Liu, G. Tkachov, E. G. Novik, C. Brüne, H. Buhmann, E. M. Hankiewicz, P. Recher, B. Trauzettel, S. C. Zhang, and L. W. Molenkamp, *Nat. Phys.* **7**, 418 (2011).
- [33] M. König, S. Wiedmann, C. Brüne, A. Roth, H. Buhmann, L. W. Molenkamp, X.-L. Qi, and S.-C. Zhang, *Science* **318**, 766 (2007).
- [34] X. Qian, J. Liu, L. Fu, and J. Li, *Science* **346**, 1344 (2014).
- [35] S. Wu, V. Fatemi, Q. D. Gibson, K. Watanabe, T. Taniguchi, R. J. Cava, and P. Jarillo-Herrero, *Science* **359**, 76 (2018).
- [36] J. Park, G. Lee, F. Wolff-Fabris, Y. Y. Koh, M. J. Eom, Y. K. Kim, M. A. Farhan, Y. J. Jo, C. Kim, J. H. Shim, and J. S. Kim, *Phys. Rev. Lett.* **107**, 126402 (2011).
- [37] V. Tayari, N. Hemsworth, I. Fakhri, A. Favron, E. Gaufrès, G. Gervais, R. Martel, and T. Szkopek, *Nat. Commun.* **6**, 7702 (2015).
- [38] Y. Zhang, K. He, C.-Z. Chang, C.-L. Song, L.-L. Wang, X. Chen, J.-F. Jia, Z. Fang, X. Dai, W.-Y. Shan, S.-Q. Shen, Q. Niu, X.-L. Qi, S.-C. Zhang, X.-C. Ma, and Q.-K. Xue, *Nat. Phys.* **6**, 584 (2010).
- [39] S. S. Hong, W. Kundhikanjana, J. J. Cha, K. Lai, D. Kong, S. Meister, M. A. Kelly, Z.-X. Shen, and Y. Cui, *Nano Lett.* **10**, 3118 (2010).
- [40] H. Tang, D. Liang, R. L. J. Qiu, and X. P. A. Gao, *ACS Nano* **5**, 7510 (2011).